Appl Phys B (2010) 99: 397–400
DOI 10.1007/s00340-010-3992-z

Applied Physics B
Lasers and Optics

RAPID COMMUNICATION

Nonclassical hydrodynamic behavior of Sn plasma irradiated with a long duration CO_2 laser pulse

Y. Tao · M.S. Tillack · S. Yuseph · R. Burdt · F. Najmabadi

Received: 22 December 2009 / Revised version: 5 March 2010 / Published online: 27 March 2010

Abstract It was found that the electron density scale length of Sn plasma irradiated with a long duration CO_2 laser pulse is much shorter than that predicted by the classical isothermal model. The experimentally observed small dominant region of in-band (2% bandwidth) 13.5-nm extreme ultraviolet (EUV) emission coincides with this constrained hydrodynamic behavior. The lower hydrodynamic efficiency may come from the strongly inhibited ablation mass and makes a CO_2-laser-produced Sn plasma suitable as an EUV radiation source.

When an intense laser pulse arrives at the surface of a solid material placed in a vacuum, a thin layer of the material is ablated, heated, and expands into vacuum due to the thermal gradient. Such hydrodynamic expansion of a laser-produced plasma has been studied for more than 40 years motivated by a wide range of applications, such as efficient compression of a pellet in laser fusion, X-ray lasers, laser ion acceleration, and short wavelength radiation sources [1]. Isothermal expansion is a well-accepted model to describe the hydrodynamic expansion of laser-produced plasma in the corona within the laser pulse duration, in which energy and material are fed by the continuously deposited laser energy near the critical density and the materials introduced from the ablation region [2]. However, the hydrodynamic expansion depends on particular experimental conditions, such as laser wavelength.

For the application of laser fusion, a lot of effort has been expended to enhance hydrodynamic efficiency in order to achieve efficient compression of the fusion pellet. It has been shown that short wavelength lasers could provide higher hydrodynamic efficiency as compared with long wavelength lasers [3]. However, for the application of radiation sources, less hydrodynamic efficiency is preferred to obtain higher radiation efficiency and less ablation mass. Recently, in-band (2% bandwidth) 13.5-nm extreme ultraviolet (EUV) emission from high Z plasma irradiated with a CO_2 laser with wavelength of 10.6 μm has been increasingly viewed as the main candidate source used in EUV lithography [4]. However, most of the previous efforts to investigate hydrodynamic behavior in intense CO_2 laser plasma interaction have focused on the preheating of the pellet induced by hot electrons, which come from nonclassical laser absorption mechanisms at the high laser intensities of interest to laser fusion [5]. The little previous efforts to characterize the thermal heat conduction inhibition in CO_2 laser plasmas interaction were done with low-density (10^{16} cm^{-3}) Z-pinch plasma [6]. In this paper, we present further understanding for the hydrodynamic behavior of a CO_2-laser-produced Sn plasma under the most favorite conditions for efficient in-band 13.5-nm EUV emission.

Experiments are carried out using a home-built master oscillator and power amplifier (MOPA) CO_2 laser system as the pumping laser pulse [7]. The CO_2 laser pulse durations are varied from 25 to 85 ns. The laser is focused with a F/6 lens onto a planar target surface at normal incidence. The

Y. Tao (✉) · M.S. Tillack · S. Yuseph · R. Burdt · F. Najmabadi
Center for Energy Research, University of California, San Diego, 9500 Gilman Drive, La Jolla, CA 92093, USA
e-mail: yetao@ucsd.edu

M.S. Tillack
Mechanical and Aerospace Engineering Department, University of California, San Diego, 9500 Gilman Drive, La Jolla, CA 92093, USA

S. Yuseph · R. Burdt · F. Najmabadi
Electrical and Computer Engineering Department, University of California, San Diego, 9500 Gilman Drive, La Jolla, CA 92093, USA

diameter of the laser focal spot is ∼100 μm. Intensities on the target for various pulse durations are almost constant at 1×10^{10} W/cm^2. A high-purity Sn slab with thickness of 2 mm is always used as the target.

A Nomarski interferometer employing an IR (1.064 μm) probe beam is used to diagnose the plasma density profile. A Nd:YAG laser with a 0.13-ns pulse duration is used as the probe beam. The probe beam passes through the EUV plasma along the target surface, i.e., at an angle of 90 degrees with respect to the target normal. The probe beam is relayed to a CCD camera by a F/5 lens with 10× magnification. Spatial resolution of the interferometer is calibrated to be better than 15 μm. The jitter is better than 5 ns. EUV images of the plasma are observed with an in-band EUV imaging system, which consists of Zr filters, a concave multilayer Mo/Si interference mirror, and a back-illuminated X-ray CCD camera. Its bandwidth (FWHM) is 0.5-nm centered at 13.5 nm. The in-band EUV imaging system is installed in the horizontal plane at an angle of 90 degrees with respect to the target normal. Its spatial resolution is better than 5 μm with a 10× magnification.

Interferograms of a Sn plasma irradiated by a CO_2 laser with pulse duration of 85 ns were observed at various delay times of 0, 30, and 60 ns with respect to the peak of the pumping laser pulse, and typical results are shown in Figs. 1a, b, and c, respectively. The laser is incident from the right hand as shown in Fig. 1. The zero point represents the peak of the CO_2 laser pulse. It is obvious as seen in Fig. 1 that the plasma expands into vacuum in both lateral and longitudinal directions. However, lateral expansion is almost constant throughout. It is also seen in Fig. 1c that at 60 ns the plasma recedes towards the initial surface in the longitudinal direction. The retreat of the plasma towards the initial target surface shows a burn-through of the expansion into a vacuum of the ablated material at a late time.

The images of in-band EUV emissions were observed with various laser pulse durations of 25, 55, and 85 ns, and typical results are shown in Figs. 2a, b, and c, respectively. Again, the laser is incident from the right hand side. The initial target surfaces are illustrated as the white dashed lines. In our experiments the times to cut the laser pulse from the oscillator of the MOPA CO_2 laser system to obtain the pulse durations of 25, 55, and 85 ns correspond to 0, 30, and 60 ns with respect to the peak of the laser pulse. So the EUV images in Figs. 2a, b, and c correspond to the interferograms shown in Figs. 1a, b, and c, respectively, except that the interferograms are taken at instantaneous times with an exposure time of 0.13 ns but the EUV image is an integration of the EUV emission generated before and at the times indicated. Hereafter, the EUV images shown in Figs. 2a, b, and c are treated approximately as taken at 0, 30, 60 ns, respectively, and the difference arising from the time-integrated measurement will be discussed later. It is worth noting that the lateral sizes of the dominant emitting region (DER, the region with an EUV intensity above the half magnitude of the maximum) of the in-band EUV emission as shown in Figs. 2a, b, and c look similar, i.e., ∼160 μm. This coincides with the observed constant lateral plasma size as shown in Fig. 1.

Plasma electron density profiles along the line of laser incidence deduced from the interferograms shown in Fig. 1 are plotted in Fig. 3. The data observed at 0, 30, and 60 ns are represented by red dots, up-faced green triangles, and down-faced blue triangles, respectively. The scale of the density is natural logarithm, its unit is the n_c of CO_2 laser, i.e.,

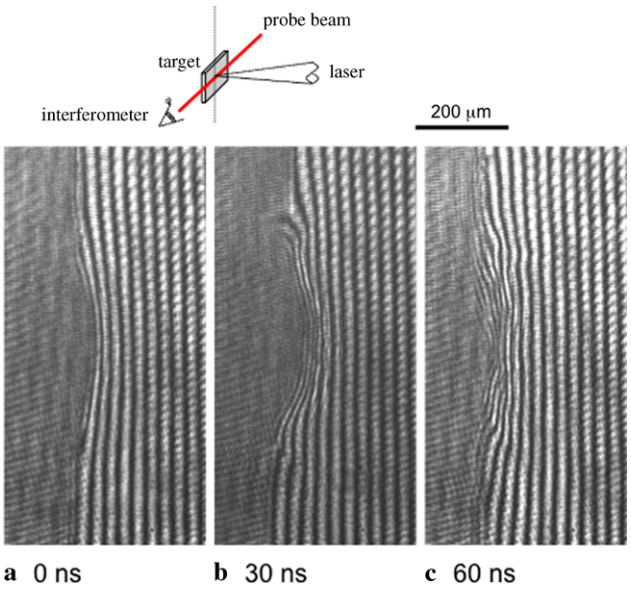

Fig. 1 Interferograms of Sn plasma irradiated with CO_2 laser pulse observed at various delay times of (**a**) 0, (**b**) 30, and (**c**) 60 ns with respect to the peak of the laser pulse

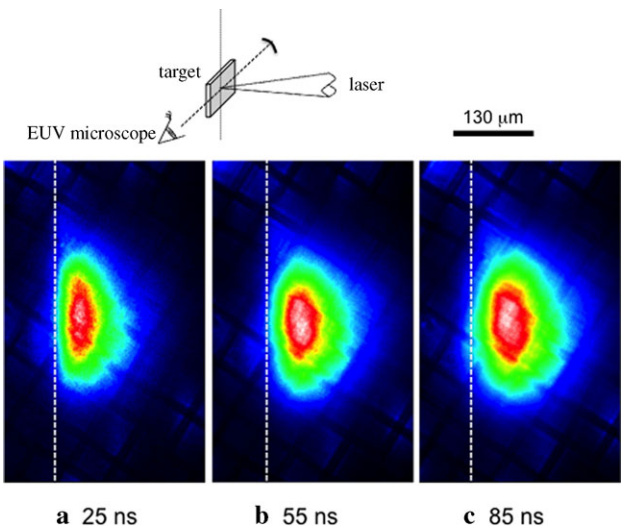

Fig. 2 In-band EUV images of Sn plasma irradiated with CO_2 laser with various pulse durations of (**a**) 25, (**b**) 55, and (**c**) 85 ns

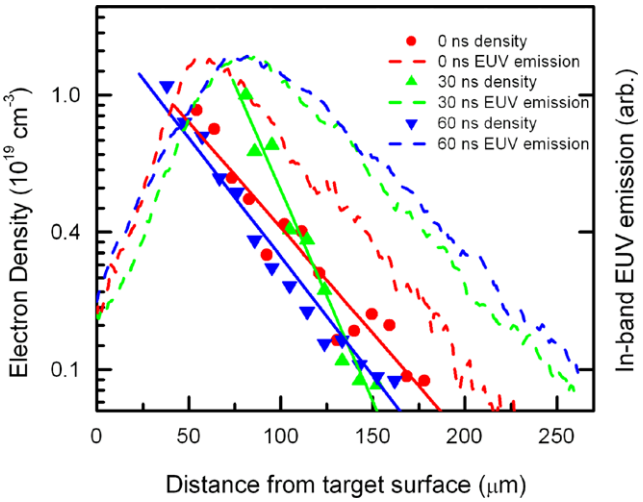

Fig. 3 Profiles of plasma density and in-band EUV emission along the line of laser incidence at various delay times 0, 30, and 60 ns

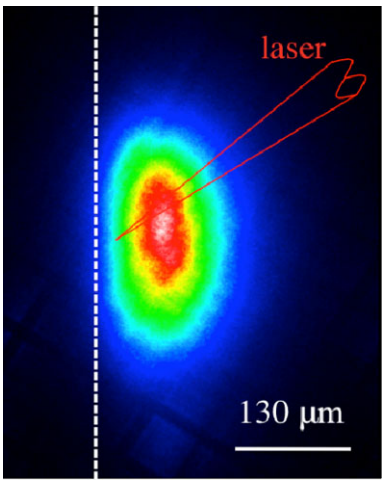

Fig. 4 In-band EUV image of Sn plasma irradiated with CO_2 laser pulse incident at an angle of 45 degrees respect to the target normal

1×10^{19} cm^{-3}. For comparison, the profiles of the in-band EUV emission along the line of laser incidence extracted from Fig. 2 are also shown in Fig. 3. The EUV emission profiles observed at 0, 30, and 60 ns are represented with the dashed lines in red, green, and blue, respectively. The EUV emission profiles are normalized according to the individual laser pulse energy. One immediate conclusion from the comparison of the profiles of the plasma density and the EUV emission is that a probe beam with wavelength of 1.064 μm is sensitive enough to obtain the plasma electron density profile in the region of interest to the generation of efficient in-band 13.5-nm EUV emission.

It is seen in Fig. 3 that at early times from 0 to 30 ns the plasma expands into the vacuum and the n_c shifts away from the initial target surface. However, at the time of 30 ns, the slope of the density profile becomes steeper as compared with that of 0 ns. It is worth noting that at a later time, i.e., 60 ns, the plasma retreats back towards the initial target surface instead of continuing to expand into vacuum. At the same time, it is also seen in Fig. 3 that the peak of the EUV emission profile also shifts into vacuum at earlier times from 0 to 30 ns, and stops at the time of 60 ns. This comparison shows that the DER of the in-band EUV appears to follow the movement of the n_c during plasma expansion. The reason for the stop of the EUV emission profile at the time of 60 ns instead of the retreat like the critical density is that as mentioned the plasma density is instantaneous but the EUV emission is time-integrated as mentioned before. It is also seen in Figs. 2 and 3 that the EUV emission profile observed at 60 ns is broader on the side closer to the initial target surface as compared with that of the 30 ns case. This broadening comes from higher EUV emission generated near the n_c surface retreating back to the target initial surface at the time of 60 ns.

In order to further clarify the location of the DER of the in-band EUV emission in CO_2-laser-produced Sn plasma, an experiment similar with that described in [8] was carried out. In [8], it has been shown that for a Nd:YAG-laser-produced Sn plasma an EUV image with a peak towards the line of laser incidence (at an angle of 45 degrees with respect to the target normal) instead of the target normal is observed due to the widely distributed laser absorption and the DER of in-band EUV emission in the corona. In the present experiment, the CO_2 laser beam is incident onto the target surface at an angle of 45 degrees with respect to the target normal and in the perpendicular plane (along the target normal). The EUV imaging system is placed in the horizontal plane and at an angle of 90 degrees with respect to the target normal. A typical EUV image of an Sn plasma irradiated by a 85-ns CO_2 laser pulse is shown in Fig. 4. It is seen that the EUV image is almost perfectly symmetric with respect to the target normal instead of the line of laser incidence, i.e., 45 degrees with respect to the target normal. This reveals that both the laser absorption and the DER of the in-band EUV emission in a CO_2-laser-produced Sn plasma is always localized near the n_c. The width of the DER of the EUV emission mainly comes from the movement of the critical density during the exposure time and the limited plasma expansion due to thermal gradient, which is always along the target normal despite the laser incident angle.

Data of the measured plasma density below the n_c in the cases of 0, 30, and 60 ns can be fitted by an exponential decay function $\exp(-x/l_s)$ with scale lengths l_s of 60 (red dashed line), 35 (green doted line), and 55 μm (blue line), respectively. An isothermal model provides a solution for the plasma electron density profile for laser-produced plasma in the corona during the laser pulse as, $n = n_c \exp(-x/l_s)$, where $l_s = c_s \tau$ is the scale length, $C_s = (ZT_e/M)^{1/2}$ is the sound speed, τ is the pulse duration, T_e is the plasma temperature, Z is the average charge state, and M is the mass

of Sn ion. Therefore, if the plasma obeys the isothermal model, the plasma density scale length can be deduced from the mentioned scaling law at various pulse durations if T_e and Z are known. It has been shown that when the optimum in-band conversion efficiency (CE) from laser to 13.5-nm EUV emission is achieved the plasma temperature should be around 30–60 eV and averaged Z should be ∼10 [9]. Since the optimized in-band CEs were observed from Sn plasmas irradiated with a CO_2 laser with pulse durations from 25 to 85 ns, it is reasonable to assume $T_e = 30$ eV and $Z = 10$ for all the plasmas with various pulse durations. The plasma scale lengths predicted by the isothermal model are 400, 880, and 1360 μm at the times of 0, 30, and 60 ns respectively. It is noted that the CO_2-laser-produced Sn plasma has a much less hydrodynamic expansion than that predicted by the isothermal model, and the deviation becomes much larger at later times.

The reason for the deviation from the classical expansion model may come from the limited material ablated by a CO_2 laser, since the energy required to keep isothermal expansion valid can be continuously compensated by the energy deposition during the laser pulse. Much less ablation mass was confirmed by an interferometry measurement of a Sn plasma driven by a 85-ns CO_2 laser as compared with that of a 7-ns Nd:YAG laser with the same laser energy. Ablation mass is closely connected with the thermal conduction between the hot n_c and the cold ablation surface. The cold material between these two surfaces is heated up and expands into the region below the n_c, and significantly contributes to the total ablation mass. This much smaller hydrodynamic efficiency suggests a much smaller flux limiter for CO_2-laser-produced Sn plasma as compared with that of a short wavelength laser. More theoretical and numerical efforts with special attention to the velocity distribution function of plasma electrons are still necessary to explain the much smaller ablation mass observed with a CO_2 laser.

This much lower hydrodynamic efficiency of a CO_2-laser-produced Sn plasma has several consequences of high radiation efficiency, weak dependence on pulse duration, and reduced debris generation, which are important for the application of a radiation source, such as an EUV lithography source. It has been shown in our previous work that a constant in-band CE, i.e., 2.6 to 3%, is obtained with a CO_2 laser with pulse durations from 25 to 100 ns [10]. The high in-band CE from a CO_2 laser to EUV emission despite reduced laser absorption due to longer wavelength can be attributed to lower hydrodynamic efficiency and the steep density profile, which reduces the reabsorption of EUV emission induced by the outer layer cold plasma [11]. And the smaller and hotter corona due to the lower hydrodynamic efficiency results in a lower laser intensity to obtain efficient 13.5-nm EUV emission. Since the small scale length outer layer cold plasma could neither significantly block the laser beam nor reabsorb the EUV light, laser absorption and EUV transport are always good for any laser pulse duration. The small ratio of the plasma density scale to the focal spot size ensures the small lateral expansion with the result that no significant laser energy is wasted even with a long duration laser pulse.

Acknowledgements This research was partially supported by Cymer Inc., KLA-Tencor Inc., EUVA in Japan, and the University of California (UC).

References

1. D. Attwood, *Soft X-Rays and Extreme Ultraviolet Radiation: Principles and Applications* (Cambridge University Press, Cambridge, 2000)
2. W.L. Kruer, *The Physics of Laser Plasma Interactions* (Addison-Wesley, Reading, 1988)
3. R.L. McCrory, R.L. Morse, Phys. Rev. Lett. **38**, 544 (1977)
4. D.C. Brandt, I.V. Fomenkov, A.I. Ershov, W.N. Partlo, D.W. Myers, N.R. Böwering, N.R. Farrar, G.O. Vaschenko, O.V. Khodykin, A.N. Bykanov, J.R. Hoffman, C.P. Chrobak, S.N. Srivastava, I. Ahmad, C. Rajyaguru, D.J. Golich, D.A. Vidusek, S. De Dea, R.R. Hou, Proc. SPIE **7271**, 727103 (2009)
5. R. Fedosejevs, I.V. Tomov, N.H. Burnett, G.D. Enright, M.C. Richardson, Phys. Rev. Lett. **39**, 932 (1977)
6. M.S. White, J.D. Kilkenny, A.E. Dangor, Phys. Rev. Lett. **35**, 524 (1975)
7. Y. Tao, M.S. Tillack, N. Amin, R.A. Burdt, S. Yuspeh, N.M. Shaikh, F. Najmabadi, Rev. Sci. Instrum. **80**, 123503 (2009)
8. Y. Tao, S. Farshad, H. Nishimura, R. Matsui, T. Hibino, T. Okuno, S. Fujioka, K. Nagai, T. Norimatsu, K. Nishihara, N. Miyanaga, Y. Izawa, A. Sunahara, T. Kawamura, Appl. Phys. Lett. **85**, 1919 (2004)
9. J. White, P. Dunne, P. Hayden, F. O'Reilly, G. O'Sullivan, Appl. Phys. Lett. **90**, 181502 (2007)
10. Y. Tao, M.S. Tillack, K.L. Sequoia, R.A. Burdt, S. Yuspeh, F. Najmabadi, Appl. Phys. Lett. **92**, 251501 (2008)
11. A. Sunahara, K. Nishihara, A. Sasaki, Plasma Fusion Res. **3**, 043 (2008)